Kalinke, Cristiane, Crapnell, Robert D ORCID logoORCID: https://orcid.org/0000-0002-8701-3933, Sigley, Evelyn, Whittingham, Matthew J, de Oliveira, Paulo R, Brazaca, Laís C, Janegitz, Bruno C, Bonacin, Juliano A and Banks, Craig E ORCID logoORCID: https://orcid.org/0000-0002-0756-9764 (2023) Recycled additive manufacturing feedstocks with carboxylated multi-walled carbon nanotubes toward the detection of yellow fever virus cDNA. Chemical Engineering Journal, 467. p. 143513. ISSN 1385-8947

https://e-space.mmu.ac.uk

Recycled additive manufacturing feedstocks with carboxylated multi-walled carbon nanotubes toward the detection of yellow fever virus cDNA

Cristiane Kalinke [a,b], Robert D. Crapnell [a], Evelyn Sigley [a], Matthew J. Whittingham [a],
Paulo R. de Oliveira [a,c], Laís C. Brazaca [d,e], Bruno C. Janegitz [c], Juliano A. Bonacin [b,*],
Craig E. Banks [a,*]

[a] *Faculty of Science and Engineering, Manchester Metropolitan University, Chester Street, M1 5GD, United Kingdom*
[b] *Institute of Chemistry, University of Campinas (Unicamp), 13083-859 São Paulo, Brazil*
[c] *Laboratory of Sensors, Nanomedicine and Nanostructured Materials, Federal University of São Carlos, Araras, 13600-970, Brazil*
[d] *Instituto de Química de São Carlos, Universidade de São Paulo, São Carlos, SP 13083-970, Brazil*
[e] *Instituto Nacional de Ciência e Tecnologia de Bioanalítica – INCTBio, Campinas, SP 13083-970, Brazil*

ABSTRACT

Recycled additive manufacturing sensing platforms are fabricated with carboxylated multi-walled carbon nanotubes (COOH-MWCNT) with exhibit enhanced electrochemical biosensor performance allowing for the enhanced direct coupling of the biorecognition element to the COOH-MWCNT for the preparation of an electrochemical genosensor for the detection of yellow fever virus cDNA. Bespoke additive manufacturing filaments was produced using recycled poly(lactic acid) (rPLA, 65 wt%), polyethylene succinate (PES, 10 wt%), carbon black (CB, 15 wt%), and COOH-MWCNT (10 wt%) which exhibits enhanced electrochemical performance over that of commercial filament. A bespoke all-in-one additive manufactured electroanalytical cell is proposed, with the working, reference and counter electrodes in addition to a modification rim that allows for the facile production of biosensors through the application of droplets. The genosensor was applied to the detection of yellow fever Virus cDNA using anodic square wave voltammetry; a linear dynamic range (LDR) of 0.5–15 μM with an R^2 of 0.9995, sensitivity of 177 ± 2 μA μM^{-1}, limit of detection (LOD) of 0.138 μM, and limit of quantification (LOQ) of 0.859 μM were obtained. This work highlights how bespoke additive manufacturing filament production can enhance biosensing platforms, whilst using recycled feedstock to improve end-product sustainability.

1. Introduction

The World Health Organization (WHO) defines the criteria required for diagnostic testing in remote or low-resource settings as: "affordability, sensitivity, specificity, user-friendliness, rapidity, and robustness, being free of equipment and being easily deliverable to end users" [1]. Additively manufactured electrochemical biosensing platforms can address the majority of these requirements due to the low-cost and portable nature of their equipment, and for being user-friendly, rapid, sensitive, and selective. Additive manufacturing - in-particular fused filament fabrication (FFF) - has seen a surge in popularity in the field of electrochemistry in recent years [2], due to the reduced costs of entry and the production of electrically conductive filament. These filaments are produced through the inclusion of conductive fillers, such as carbon black (CB), into the thermoplastic matrix, such as poly(lactic acid) (PLA). Additive manufacturing allows for the production of electrodes [3] and electrochemical equipment [4] on-site with bespoke geometries, significantly lower manufacturing timescales, reduced material waste and marginal costs. The digital nature of additive manufacturing also allows for the production or modification of designs anywhere in the world, with printing able to happen *in situ*, wherever access to a printer and filament is available.

Current additive manufacturing electrochemical biosensors in literature commonly utilise the commercially available filaments ProtoPasta or BlackMagic, which are based on the conductive fillers CB or graphene, respectively. To improve the performance of additive

manufacturing electrochemical systems, bespoke filaments that offer significant electrochemical improvements in regards to energy storage [5] and electroanalysis [6] are being reported, whilst also utilising recycled polymers. This improved sustainability in a additive manufacturing electrochemistry further enhances its appeal, as it aligns with the UN's Sustainable Goal #12 – Ensure sustainable consumption and production patterns, and the EU's "Plastics in a Circular Economy" policy [7].

Multi-walled carbon nanotubes (MWCNT) embedded filaments have been reported previously, with groups utilising them in low loadings (0.25–7 wt%) to improve the mechanical properties of 3D-printed pieces [8]. Some examples have recently been reported for the use of MWCNTs to improve the electrical conductivity of filaments. For example, Vidakis *et al.* [9] utilised 10 wt% in a polyamide filament, and Ivanov *et al.* [10] used a combination of graphene nanoplatelets and MWCNT at a total filler of 6 wt% in a PLA filament. These systems, although electrically conductive, do not come close to the required conductivity for electrochemical applications. For example, commonly used commercial filament Protopasta quotes a resistance across 10 cm as 2–3 kΩ for their 1.75 mm filament [11]. Ghosh and co-workers [12] reported filaments combining activated charcoal, MWCNT and MoS2 (22.7, 4.5 and 9.0 wt % respectively) for photo and electrochemical energy conversion and storage, but the inclusion of MoS2, low loading of MWCNT and inclusions of poly(ethylene glycol) [5] makes the system unsuitable for biosensing applications.

There have been numerous publications on the electrochemical determination of virus diseases [13–17], in particular for emergent diseases, such as zika and dengue [18,19], Ebola [20] and SARS-CoV-2 in recent years [21–31]. This increased coverage stemmed from the effect this outbreak had on both industrialised countries and low-resource areas. These low-resource settings continue to suffer from increased outbreaks of neglected diseases not seen as commonly elsewhere, such as the outbreak of yellow fever in Africa with high case-fatality [32]. Yellow fever is a disease considered endemic in tropical regions; however, the demographic expansion to other countries has been increasing in recent years, already being considered an emerging disease in South America and Africa [33,34]. The disease - normally transmitted by arthropods, such as the *Aedes aegypti* mosquito and ticks - causes a haemorrhagic viral fever in addition to other symptoms such as headaches, malaise, rash, nausea, vomiting, and diarrhoea. This can evolve rapidly to multiple organ failure syndrome, causing death [34]. Despite the existence of a highly effective vaccine, yellow fever still affects thousands of people each year [35]. Continuous global improvements in testing preparedness are essential for future outbreaks of any kind, in both industrialised countries and low-resource settings [1].

In this work, we propose the development of a novel additive manufacturing filament that still utilises recycled PLA and CB, but additionally embeds carboxylated MWCNT (COOH-MWCNT, 10 wt%) within the matrix. This composition retains the excellent flexibility and printability of the filament, whilst improving the electrochemical performance and allowing for the enhanced direct coupling of the biorecognition element to the COOH-MWCNT for the preparation of an electrochemical genosensor for the detection of yellow fever virus cDNA. Additionally, due to the availability, flexibility, low-cost and low-waste advantages of FFF as a manufacturing technology, this work offers an alternative route the supply of biosensors for low-resource environments in the future.

2. Experimental section

2.1. Chemicals

All chemicals used were of analytical grade and were used as received without any further purification. All solutions were prepared with deionised water of resistivity not less than 18.2 MΩ cm from a Milli-Q Integral 3 system from Millipore UK (Watford, UK).

Hexaamineruthenium (III) chloride (RuHex, 98%), ferrocene methanol (FcMeOH, 97%), poly(ethylene succinate) (PES, MW:10,000) sodium hydroxide (>98%), potassium chloride (99.0–100.5%), bovine serum albumin (BSA, >98%), N-(3-dimethylaminopropyl)-N'-ethyl-carbodiimide hydrochloride (EDC, >99%), N-hydroxysuccinimide (NHS, 98%), human serum (AB plasma) and phosphate buffered saline (PBS) tablets were purchased from Merck (Gillingham, UK). Carbon black (Super P®, >99+%) was purchased from Fisher Scientific (Loughborough, UK). Short (0.5–2.0 μm) and long (10–30 μm) carboxylated multi-walled carbon nanotubes (COOH-MWCNT, 10–20 nm outer diameter) were purchased from Cheap Tubes (VT, United States). Recycled poly(lactic acid) (rPLA) was purchased from Gianeco (Turin, Italy). The DNA capture probe (TTGGATCCTGCACGACAACAGAA) was purchased from Exxtend Biotecnologia (Paulínia, Brazil). Short and long sequences of Yellow Fever virus cDNA (YFV, TTCTGTTGCGTGCAG-GATCCA, GTGGAGAAGCAGGGCAGATGAGATCAATGCCATTTTTGAGG AAAACGAG) and Dengue virus cDNA (DENV, CAGGCCGATAGTG GTTGCGTTGT, TGGGAATTGTGACACTGTATTTGGGAGTCATGGTGCA GGCCGATAGTGG) were purchased from Exxtend Biotecnologia (Paulínia, Brazil). All sequences were modified on 5′ end with a C-6 spacer and amino groups. Commercial conductive PLA/carbon black filament (1.75 mm, ProtoPasta, Vancouver, Canada) was purchased from Farnell (Leeds, UK). Commercial non-conductive PLA filament (1.75 mm, galaxy silver, Prusament) was purchased from Prusa Research (Prague, Czech Republic).

2.2. MWCNT-COOH recycled filament production

Prior to any mixing or filament production all rPLA was dried in an oven at 60 °C for a minimum of 2.5 h, which removed any residual water in the polymer. Conductive polymer compositions were all prepared using a mixing chamber of 63 cm³, to produce two (long and short) compositions of COOH-MWCNT embedded filament. The filaments were produced using 65 wt% rPLA, 10 wt% PES, 15 wt% CB, and 10 wt% COOH-MWCNT. As a benchmark in this work, alongside the commercial PLA/CB, a conductive filament was produced without MWCNT, comprising of 65 wt% rPLA, 10 wt% PES, and 25 wt% CB. The filament components were mixed in a heated chamber (170 °C) fitted with Banbury rotors at 70 rpm for 5 min, using a Thermo Haake Poydrive dynameter fitted with a Thermo Haake Rheomix 600 (Thermo-Haake, Germany). The collected mixes from the Rheomix were allowed to cool to room temperature before being granulated to create a finer granule size using a Rapid Granulator 1528 (Rapid, Sweden). The granulated sample was collected and processed through the hopper of a EX6 extrusion line (Filabot, VA, United States). The EX6 was set up with a single screw and had four set heat zones of 60, 190, 195 and 195 °C respectively. The molten polymer was extruded from a 1.75 mm die head, pulled along an Airpath cooling line (Filabot, VA, United States, through an inline measure (Mitutoyo, Japan) and collected on a Filabot spooler (Filabot, VA, United States). The filament was then ready to use for Additive Manufacturing (AM).

2.3. Additive manufacturing

All computer designs and.3MF files seen throughout this manuscript were produced using Fusion 360® (Autodesk®, CA, United States). These files were sliced and converted to.GCODE files using the open-source software PrusaSlicer (Prusa Research, Prague, Czech Republic) for the additively manufactured working electrodes (AMEs), and idea-Maker (RAISE3D, CA, United States) for the electrochemical cell with embedded counter and reference electrodes.

The AMEs were 3D-printed using fused filament fabrication (FFF) technology on a Prusa i3 MK3S+ (Prusa Research, Prague, Czech Republic). All AMEs were printed using a 0.6 mm nozzle with a nozzle temperature of 215 °C, 100% rectilinear infill, 0.15 mm layer height, and print speed of 70 mm s^{-1}.

The electrochemical cell with embedded counter and reference electrodes were produced on a RAISE3D E2 independent dual-extruder (IDEX) 3D-printer. The non-conductive filament was loaded to the left-hand extruder and the conductive filament loaded to the right extruder. The cells were printed with a bed temperature of 55 °C, nozzle temperatures of 205 °C, 0.4 mm extrusion width, 0.2 mm layer height, shell width of 1 mm, left infill of 10% and right infill of 100%, with an print speed of 60 mm s^{-1}.

2.4. Physiochemical characterisation

X-ray Photoelectron Spectroscopy (XPS) data were acquired using an AXIS Supra (Kratos, UK), equipped with a monochromated Al X-ray source (1486.6 eV) operating at 225 W and a hemispherical sector analyser. The equipment was operated in fixed transmission mode with a pass energy of 160 eV for survey scans and 20 eV for region scans with the collimator operating in slot mode for an analysis area of approximately 700 × 300 μm, the FWHM of the Ag $3d_{5/2}$ peak using a pass energy of 20 eV was 0.613 eV. Before analysis, each sample was ultrasonicated for 15 min in propan-2-ol and then dried for 2.5 h at 65 °C as this has shown - in our unpublished data - to remove excess contamination and therefore minimise the risk of misleading data. The binding energy scale was calibrated by setting the C-C sp^3 C 1 s peak to 285.0 eV; this calibration is acknowledged to be flawed [36], but was nonetheless used in the absence of reasonable alternatives, and because only limited information was to be inferred from absolute peak positions.

Scanning Electron Microscopy (SEM) measurements were recorded on a Supra 40VP Field Emission (Carl Zeiss Ltd., Cambridge, UK) with an average chamber and gun vacuum of 1.3 × 10^{-5} and 1 × 10^{-9} mbar, respectively. Samples were mounted on the aluminium SEM pin stubs (12 mm diameter, Agar Scientific, Essex, UK). To enhance the contrast of these images, a thin layer of Au/Pd (8 V, 30 s) was sputtered onto the electrodes with the SCP7640 from Polaron (Hertfordshire, UK) before being placed in the chamber.

Raman spectroscopy was performed on a Renishaw PLC in Via Raman Microscope controlled by WiRE 2 software at a laser wavelength of 514 nm.

2.5. Electrochemical experiments

All electrochemical measurements were performed on an Autolab M204 potentiostat controlled by NOVA 2.1.5 software (Utrecht, the Netherlands). The electrochemical characterisation of the bespoke filament and comparison to the benchmarks were performed using lollipop design (Ø 3 mm) electrodes alongside an external commercial Ag|AgCl reference electrode and a nichrome wire counter electrode. The detection of Yellow Fever Virus (YFV) target sequence was performed using a complete AM cell, using a 3D-printed working, reference, and counter electrodes. It should be noted all reference and counter electrodes were printed from the commercially purchased conductive CB/PLA filament. All solutions of RuHex and FcMeOH were prepared using deionised water of resistivity not less than 18.2 MΩ cm from a Milli-Q system (Merck, Gillingham, UK) and were purged of O$_2$ thoroughly using N$_2$ prior to any electrochemical experiments.

Activation of the AMEs, when applicable, was achieved through incubation of a droplet of 0.5 M NaOH onto the surface of the electrode for 30 min, followed by washing with deionised water and drying with N$_2$.

2.6. Biosensor production

For the modification of the biosensor, EDC/NHS coupling was used for the stable immobilization of the YFV cDNA capture sequence through the carboxyl functionalization. The incubation with a solution of EDC (5.0 mM) and NHS (1.0 mM) in PBS buffer (pH = 5.0) was carried out by adding a 10 μL drop on the working electrode for 1 h. The capture sequence immobilization (1.0 μmol L^{-1} in PBS buffer pH = 7.4, for 1 h)

was carried out in a similar way, occurring due to binding between amino groups present on the modified capture probe and carboxylic groups of the sensor. A 1.0 wt% BSA solution was then added to the working electrode for 30 min to mitigate any nonspecific interactions with the carboxyl groups. The hybridization between the immobilized capture sequence and the YFV target sequence was conducted for 1 h. Different concentrations of target prepared in PBS buffer (pH = 7.4) were evaluated. After each modification step, the electrode was washed with PBS buffer and dried under N$_2$. Linear sweep voltammetry (LSV) and square wave voltammetry (SWV) measurements were carried out in presence of 1.0 mmol L^{-1} FcMeOH as the electrochemical probe.

2.7. Selectivity and real sample analysis

Anodic and cathodic SWV measurements were performed for human serum sample before and after the YFV cDNA target sequence hybridization at three levels of concentration (1.0, 5.0, and 10 μM). The selectivity of the YFV genosensor was tested against dengue virus (DENV) cDNA, which present similar symptoms and it could be confused with YFV. Anodic and cathodic SWV measurements were conducted after the hybridization reaction with 10 μM DENG cDNA target sequence.

3. Results and discussion

The use of additive manufacturing can transform the production and delivery of electrochemical biosensors due to its versatility, low wastage, and low cost. To meet requirements regarding biosensor production - including increased sensitivity and reproducibility - new conductive filaments must be designed and produced. Herein, we show the production, characterisation and application of a new conductive filament from recycled poly(lactic acid) (rPLA), poly(ethylene succinate) (PES), carbon black (CB), and short and long carboxylated multi-walled carbon nanotubes (S-COOH-MWCNT, L-COOH-MWCNT) toward the production of a genosensor for Yellow Fever virus cDNA.

3.1. Production and characterisation of functional recycled filament

The production of the bespoke filaments consisting of 65 wt% rPLA, 10 wt% PES, 15 wt% CB and 10 wt% MWCNT is shown schematically in Fig. 1A. Prior to anything else, all rPLA was dried in an oven at 60 °C for a minimum of 2 h to remove any residual water [37]. For this work three bespoke filaments were produced, keeping the conductive carbon-based filler content stable at 25 wt%, and the plasticiser content stable at 10 wt%. The first composition comprised of 25 wt% CB and was used as a benchmark alongside the commercially purchased conductive filament Protopasta. The two filaments primarily under investigation consisted of 15 wt% CB and 10 wt% S-COOH-MWCNT or L-COOH-MWCNT. The components for each bespoke filament were mixed at 170 °C for 5 min, cooled, shredded, and passed through a single-screw extruder to produce filaments of 1.75 mm diameter. Fig. 1B shows photographs of the filament produced using L-COOH-MWCNT, highlighting the flexibility of the obtained filament due to the inclusion of the plasticiser PES, which has been shown to help produce filament with high-loadings of carbon [6].

Thermogravimetric analysis (TGA) was performed on the bespoke filaments and the component polymeric parts, presented in Fig. 1C. This analysis gives important information about the historical thermal processing of the rPLA, how subsequent processing into the conductive filament affects its thermal stability, what effect the PES plasticiser has on the thermal properties of the produced filaments, and importantly to determine the mass of conductive filler present in each composite. The TGA results are presented in Table 1, where the average degradation onset temperatures, average final masses and average conductive filler content are summarised. It can be seen in Table 1 that the PLA and PES have significantly different thermal stabilities, where PLA has an onset
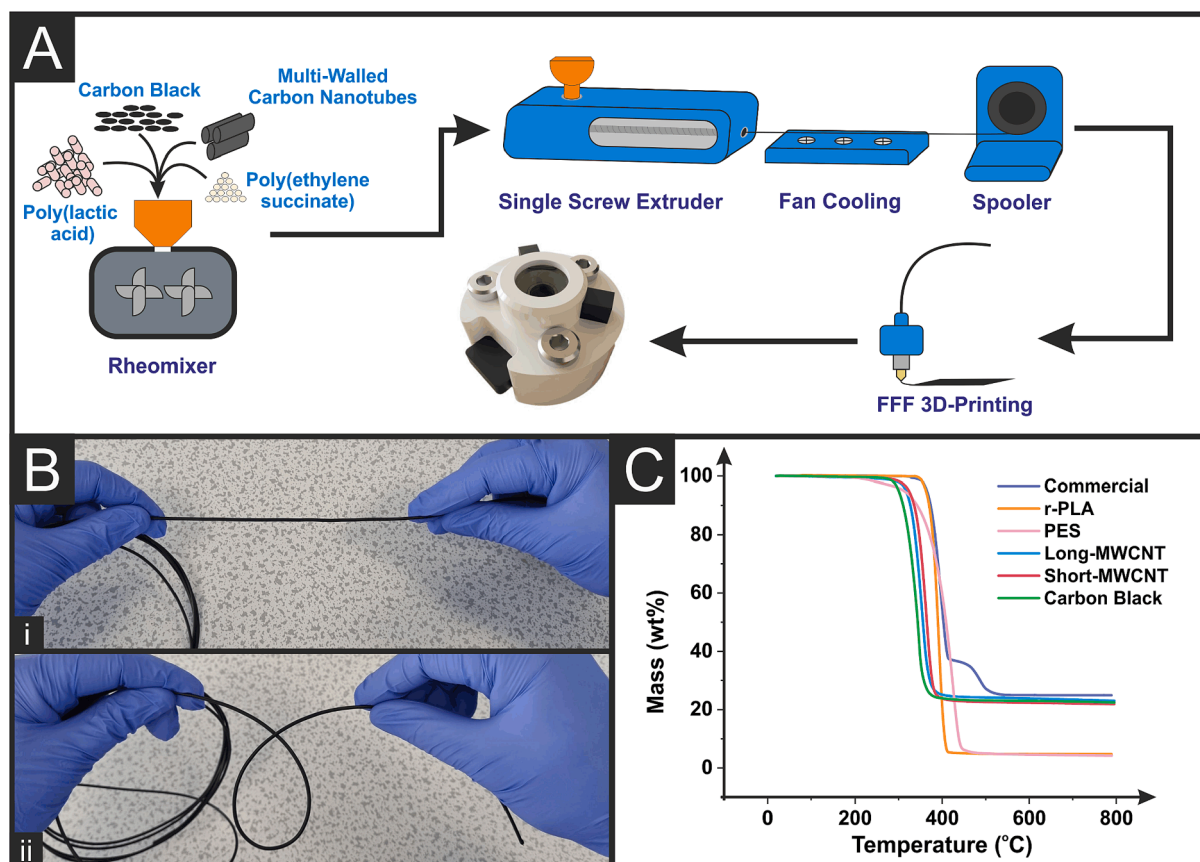
Fig. 1. A) Schematic for the production of filament in this work containing 65 wt% r-poly (lactic acid), 10 wt% poly(ethylene succinate), 15 wt% carbon black, and 10 wt% carboxylated multi-walled carbon nanotubes. **B)** Photographs of the long-COOH-MWCNT filament **i)** straightened and **ii)** bent, highlighting the flexibility of the filament. **C)** Thermogravimetric analysis of the different filaments explored in this work and their key component parts.

Table 1

Thermogravimetric analysis of the different components and filaments used throughout this work. Highlighting the average onset temperatures, average final masses, and the conductive filler contents where applicable. Uncertainties in the values represent the standard deviation from three separate measurements.

Sample	Onset Temp 1 (°C)	Onset Temp 2 (°C)	Final Mass (wt%)	Filler Content (wt%)
Natural PLA	305 ± 5	N/A	3 ± 2	N/A
PES	198 ± 1	N/A	1 ± 1	N/A
Commercial	304 ± 2	436 ± 4	24 ± 2	21 ± 3
rPLA/CB	230 ± 4	N/A	22 ± 1	19 ± 3
rPLA/CB/S-COOH-MWCNT	219 ± 4	N/A	23 ± 1	20 ± 3
rPLA/CB/L-COOH-MWCNT	219 ± 1	N/A	23 ± 1	20 ± 3

temperature of 305 ± 5 °C compared to the 198 ± 1 °C measured for the PES sample. The effect of this on the final filament can be seen when comparing the three bespoke compositions to the commercially purchased conductive filament. The commercial filament presents a similar first onset temperature to the PLA of 304 ± 2 °C but shows an additional decomposition onset, speculated to be the unknown plasticiser listed by the manufacturer [11]. In comparison, all bespoke filament exhibit degradation onset temperatures significantly lower, with the 25 wt% CB filaments at 230 ± 4 °C, and both COOH-MWCNT filaments exhibiting an onset temperature of 219 °C (± 4 and ± 1 °C for the short and long MWCNT, respectively). The higher onset temperatures of the bespoke filaments compared to the pure PES is proposed to be due to some

thermal stabilisation gained by the composite through the incorporation of carbon black [38] and MWCNT [39], where the particles themselves act as physical barriers for gas diffusion out of the polymer, slowing the rate of decomposition [40].

The conductive filler contents listed within Table 1 are noticeably lower than the final mass obtained for each composite. This is due to the charring of the PLA in the nitrogen atmosphere, leaving residual mass in the sample pan, which can be seen within the pure rPLA sample run. Therefore, filler content is taken as the final average mass of the composite minus the average charred mass of the rPLA. Using this method, the filler content of the commercial sample was found to be 21 ± 3 wt%, which shows good agreement with the 21.43 wt% filler listed by the manufacturer [11]. In this work, to produce the optimal balance between printing and electrochemical performance, the conductive filler content was reduced from previous works [5,6], with the filler contents calculated at 19 ± 3 wt% for the CB filament, and 20 ± 3 wt% for the S-COOH-MWCNT and the L-COOH-MWCNT filaments.

For the physiochemical and electrochemical characterisation of additively manufactured electrodes (AMEs) printed from these filaments, they were printed into simple lollipop shapes, Figure S1A. These were printed with a 5 mm disc as the working electrode and a 18×1 mm stem, keeping the connection length as short as possible to allow for easy use, but also the best electrochemical performance [41]. XPS C 1 s spectra, Raman spectra and SEM images for the S-COOH-MWCNT and L-COOH-MWCNT are presented in Fig. 2. XPS analysis was performed to investigate the chemical composition of the AMEs as printed and then after activation. In comparison to previous works [5,6,42], the electrodes herein were activated simply through incubating a droplet of NaOH (0.5 M) on the electrode surface for 30 min, as this aligned with the facile biosensor production desired. Figure S3 shows the XPS C 1 s
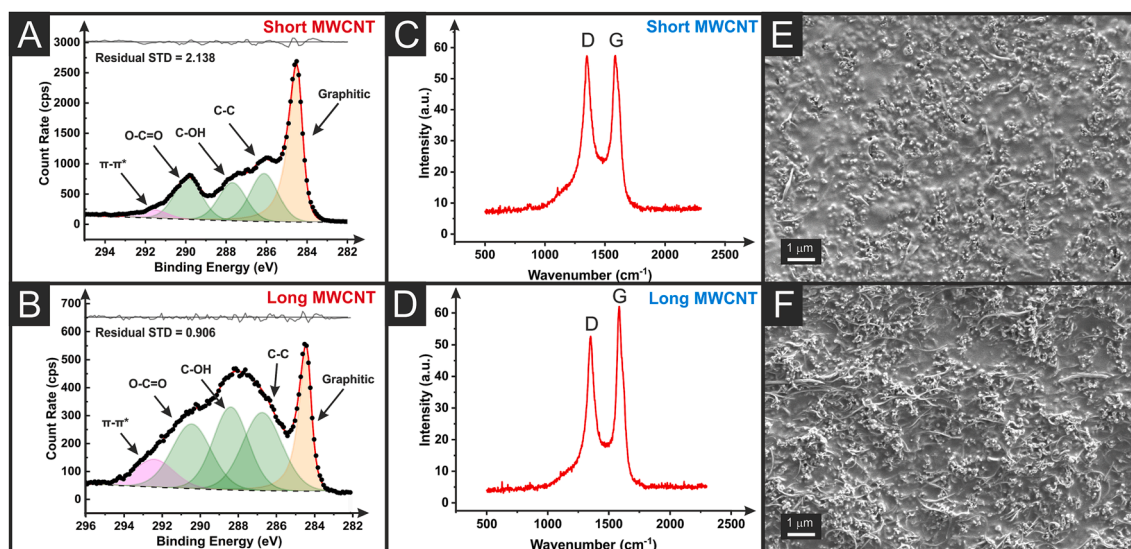
Fig. 2. A) XPS C 1 s analysis, **B)** Raman analysis, and **C)** SEM image of the activated AME made with short-COOH-MWCNT. **D)** XPS C 1 s analysis, **E)** Raman analysis, and **F)** SEM image of the activated AME made with long-COOH-MWCNT.

spectra for the as-printed AMEs, with both the short and long MWCNT samples showing a small asymmetric peak, which was assigned as sp^2 graphitic carbon and used to calibrate the rest of the spectrum by setting its centra to 284.5 eV in accordance with graphitic carbon. Both as-printed AMEs show three additional major peaks in the C 1 s spectrum of similar peak heights and increasing in binding energy. These are attributed to the increasingly oxidised carbon environments in PLA and PES.

For the activated AMEs, Fig. 2A and B, it can be seen that there is a large increase in magnitude of the graphitic sp^2 carbon peak, which is again set as 284.5 eV and used to calibrate the rest of the spectrum. Once more there are three carbon environments present of an increasingly oxidised nature, corresponding to both PLA and PES. In addition to these peaks, there is a small peak required at even higher binding energies consistent with π-π* transitions in graphitic materials. The large increase in magnitude of the graphitic peak and appearance of the π-π* transition peak gives evidence toward the successful activation of the AMEs through stripping of the PLA and PES, revealing enhanced amounts of the CB and MWCNTs present in the composite.

Raman analysis was performed on these samples, Fig. 2 C and D, showing the characteristic D and G bands for MWCNTs present at ~1300 and 1600 cm^{-1}. It can be seen that there is an increase in the intensity of the G band present in the long MWCNT compared to the short MWCNT. This is expected as the G band originates from the sp^2 bonded graphitic carbon and the D band corresponds to the open end (or defects) of a carbon nanotube, of which there is expected to be more for the shorter MWCNT in the same mass [43,44]. The increased length of the MWCNT and presence of them on the surface is confirmed through SEM imaging, Fig. 2 E and F. Nanotube structures can clearly be seen on the SEM images alongside the small spherical particulates which correspond to the CB particles in the composite. Fig. 2F highlights the long COOH-MWCNTs, showing a high density of MWCNT that bridge along the AME giving rise to its excellent conductivity. Following this, it is important to characterise the AMEs against common redox probes to help elucidate their electrochemical properties before use in the genosensor.

3.2. Electrochemical characterisation of additive manufacturing electrodes (AMEs)

All electrochemical characterisation of the AMEs in this work was performed using the lollipop electrodes outlined in Figure S1 A,

alongside a nichrome wire counter electrode (CE) and commercial Ag| AgCl reference electrode (RE). This was done to maintain consistency and ensure all electrochemical effects seen were due to the AME and not variations in the print or composition of the CE or RE. The four lollipop electrodes studied were printed from commercial conductive filament, and three lab-made bespoke filaments consisting of 25 wt% CB, or 15 wt% CB + 10 wt% S-COOH-MWCNT, or 15 wt% CB + 10 wt% L-COOH-MWCNT. Initial electrochemical characterisation was performed for the as-printed AMEs against the near-ideal outer sphere redox probe hex-aamineruthenium (III) chloride (RuHex) [45]. Fig. 3A shows the CV obtained at 25 mv s-1 with and without RuHex (1 mM, 0.1 M KCl) for AMEs printed from each filament. It is evident that the lab-made CB filament presents significantly lower peak-to-peak (ΔEp) separation when compared to the commercial CB filament, but both produce similar peak currents, even though TGA analysis indicated that the lab-made filament had slightly less conductive filler. In contrast, both filaments containing MWCNT showed significantly increased peak currents, in addition to an improved ΔEp. Scan rate studies in these conditions allowed the determination of the heterogeneous electrochemical rate constant (k_o) and the real electrochemical surface area (Ae) [46], summarised in Table S1. It can be seen that all bespoke AMEs showed significant improvements over the commercial one in all categories with the L-COOH-MWCNT AME producing a $k^0 = (1.37 \pm 0.35) \times 10^{-3}$ cm s^{-1} compared to $0.46 \pm 0.10 \times 10^{-3}$ cm s^{-1} for the commercial filament. To further see how the performance of the bespoke AMEs compared to the commercial, EIS was performed in RuHex. Fig. 3B shows the Nyquist plots obtained, where it can be seen that the bespoke filaments offer significantly lower charge-transfer resistance (R_{CT}). Through fitting of the Nyquist plots with an appropriate Randles circuit, the R_{CT} was quantified; with the commercial AME producing a value of 832 ± 176 Ω, compared to 183 ± 4 Ω for the S-COOH-MWCNT and 106 ± 4 Ω for the L-COOH-MWCNT. This gives evidence toward the bespoke MWCNT filaments having far better electrochemical characteristics and being significantly more consistent.

To further study the electrochemical characteristics of the AMEs, scan rate studies were performed before and after activation in ferro-cenemethanol (1 mM, 0.1 M KCl). The cyclic voltammograms at 25 mV s^{-1} with and without the presence of ferrocenemethanol are presented in Fig. 3C, and the corresponding Randles–Ševčík plot obtained from the study is shown in Fig. 3D. From the CVs it can be seen that again the filament containing the MWCNT significantly outperform the commercial filament in terms of both ΔE$_p$ and obtained peak current. The
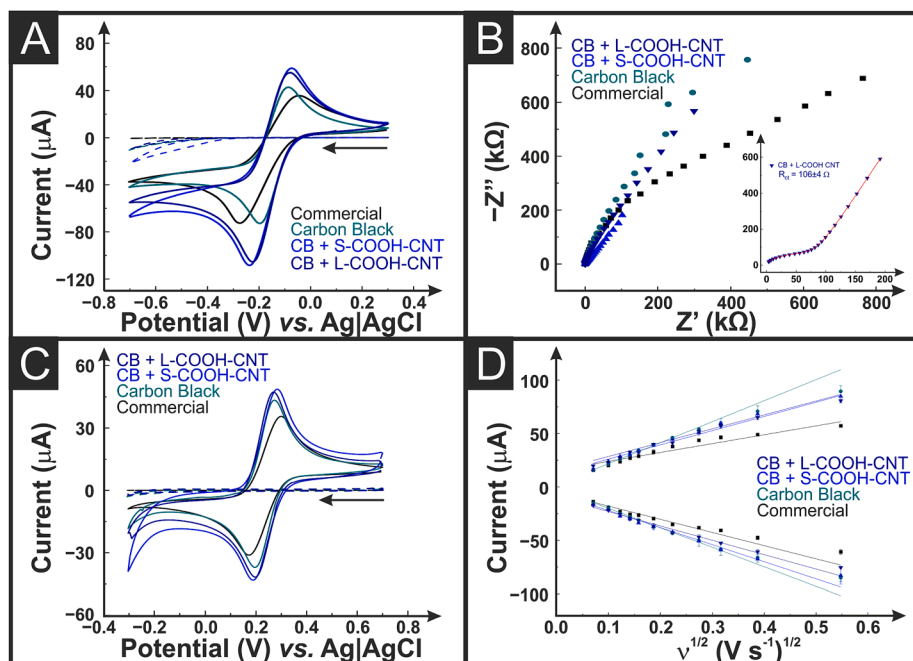
Fig. 3. A) Cyclic voltammograms (25 mV s^{-1}) with and without the presence of hexaamineruthenium (III) chloride (1 mM, 0.1 M KCl) for AMEs printed from the four different filaments. **B)** Nyquist plot for each AME in hexaamineruthenium (III) chloride (1 mM, 0.1 M KCl). Inset enlarged Nyquist plot and fit for the long-COOH-MWCNT filament. **C)** Cyclic voltammograms (25 mV s^{-1}) with and without the presence of ferrocenemethanol (1 mM, 0.1 M KCl) for AMEs printed from the four different filaments. **D)** A plot of peak current versus the square-root of the scan rate comparison for the AMEs printed with the three bespoke filaments and the commercial filament. Performed against an Ag|AgCl reference electrode and nichrome wire counter.

summary of the data obtained from this study is presented in Table 2. Improvements in every AME can be seen after activation by incubation in NaOH, with the L-COOH-MWCNT AME performing the best in every category. This AME produced a k^0 of $(1.85 \pm 0.42) \times 10^{-3}$ cm s^{-1} and an electrochemically active area of (2.11 ± 0.03) cm^2 compared to $(1.19 \pm 0.19) \times 10^{-3}$ cm s^{-1} and (1.35 ± 0.02) cm^2 for the commercial filament. The improved electrochemical performance and presence of carboxyl groups on the surface of the electrode made the L-COOH-MWCNT filament most suited for use in the genosensor.

3.3. Design and production of bespoke recycled cell

CAD (computer aided designs) images of the AM electrochemical cell for the genosensor are presented in Fig. 4, with multiple perspectives highlighting the key aspects of the design. The design was split into three separate prints, shown in Fig. 4 A: the working electrode (WE) from the bespoke conductive filament, the top part of the cell with reference and

Table 2
Comparison of the calculated heterogenous electron rate constant, k^o and electroactive area for AMEs printed using the four filaments before and after activation. Calculated using ferrocenemethanol (1 mM, 0.1 M KCl) and a geometric area of 0.236 cm^2. Uncertainties in the values represent the standard deviation from three separate measurements.

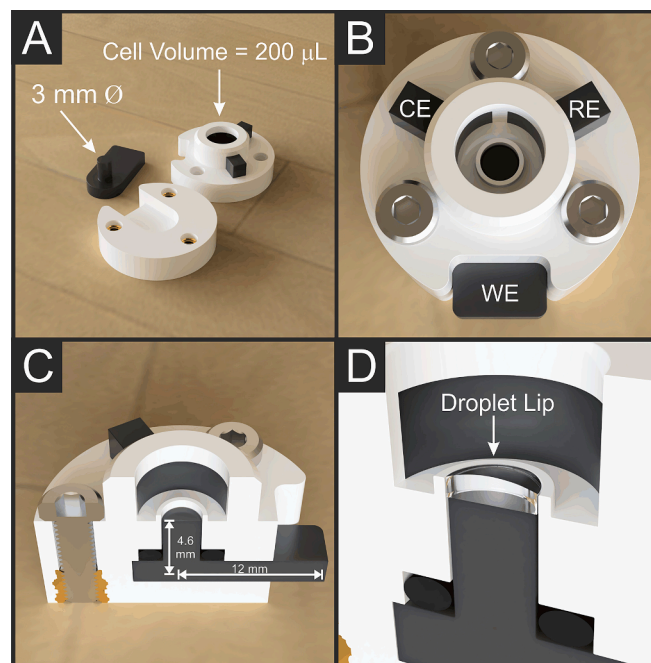| AME Filament		k^0 ($\times 10^{-3}$ cm s^{-1})	A_{real} (cm^2)	A_{real} (%)
Commercial	As printed	0.66 ± 0.10	0.64 ± 0.04	64 ± 4
CB	Activated	1.19 ± 0.19	1.35 ± 0.02	135 ± 2
r-PLA, 25% CB	As printed	1.53 ± 0.50	1.17 ± 0.04	117 ± 4
	Activated	1.83 ± 0.44	1.76 ± 0.04	176 ± 4
r-PLA, 15 % CB	As printed	1.47 ± 0.31	0.90 ± 0.02	90 ± 2
10% S-COOH-MWCNT	Activated	1.70 ± 0.35	2.04 ± 0.02	204 ± 2
r-PLA, 15 % CB	As printed	1.74 ± 0.58	0.82 ± 0.04	82 ± 4
10% L-COOH-MWCNT	Activated	1.85 ± 0.42	2.11 ± 0.03	211 ± 3

Fig. 4. A) CAD Images of the cell used for the genosensor, including **A)** separate component parts including separate working electrode, bottom cell with heat-set inserts, and top cell with embedded reference and counter electrodes. **B)** Top view of the combined cell showing the working electrode in the base with counter and reference on each side. **C)** Cut through of the cell showing the dimensions of the working electrode. **D)** Isometric cut through highlighting the embedded lip of the cell to improve droplet immobilisation.

counter electrodes embedded into the print, and the base plate which fits the WE and has heat-set inserts placed within to allow for secure fastening to avoid possible leaks. This design allowed the top and bottom parts of the electrochemical cell to be identical for all different compositions of the working electrode, with both the reference and counter electrodes printed using the commercially available conductive filament. The top part of the cell was designed with both the reference and

counter electrodes having the same size (3x WE surface area). This also avoided any possibility of variation happening in the electrochemistry due to using different materials or sizes as the reference and counters. This electrochemical cell was designed to hold a small sample volume of 200 μL, meaning that multiple measurements could be done from a single blood sample. The working electrode was printed as a t-shape as seen previously [6], which allowed for the simple sealing of the system with an O-ring. The WE had an overall horizontal connection length of 12 mm and vertical of 4.6 mm (Fig. 4 C), which was the smallest that was reproducibly printable, keeping the connection length as short as possible due to the effect this can have on the electrochemical response of AMEs [41]. Additionally, on the top part of the electrochemical cell a small lip was added around where the working electrode sat, Fig. 4D. This is an important addition that allows for the reproducible application of droplets used in activation and biosensor production, stoppling solution from spilling onto the surrounding non-conductive PLA. This cell was then applied to the production and use of the genosensor towards Yellow Fever Virus cDNA.

3.4. Biosensor production, characterisation, and application

The genosensor for the detection of Yellow Fever Virus target sequence was constructed through a facile droplet methodology as outlined in Fig. 5A, utilising the specially designed lip in the electrochemical cell for holding the droplets in position over the WE. The WE is placed inside the electrochemical cell and incubated with a droplet of NaOH (0.5 M) for 30 min to activate the AME surface. Following this, EDC/NHS coupling of the DNA capture probe is performed, linking the amine terminated probe to the carboxyl groups on the AME surface. The remaining free surface is then blocked with BSA and the sensing platform is ready to use. Tracking of these AME modification steps is shown in Fig. 5B through anodic square wave voltammograms (SWV) in presence of ferrocenemethanol (1.0 mM FcMeOH) as the redox probe. Decreases in the obtained peak current can be seen between the bare AME surface, for the attachment of the DNA capture probe, blocking of the surface with BSA and finally for incubation with the DNA target. Due to

the activation of the AME surface using NaOH, and the nature of the carbon fillers used in their production, carboxyl groups are expected to be in all samples. The biosensor modification process was therefore applied to all AMEs, with the overall peak current change after incubation with 1 μM Yellow Fever Virus cDNA plotted in Fig. 5C. As expected, there is a change in the current for all AMEs but a significantly larger change for the COOH-MWCNT systems due to the presence of the already carboxylated MWCNTs. In this case, again the L-COOH-MWCNT AMEs produced the biggest change in current with excellent reproducibility and was therefore chosen for further tests.

The detection of Yellow Fever virus target sequence in buffered solution with the L-COOH-MWCNT AMEs was tested using anodic linear sweep voltammetry (ALSV, Figure S3A), anodic square wave voltammetry (ASWV, Fig. 6A) and cathodic square wave voltammetry CSWV, Figure S3B). In all cases there is a clear decrease in the measured peak currents with the increased concentration of the target sequence. The key analytical parameters obtained for each detection methodology are presented in Table S2, where the ASWV gave the best performance. Using ASWV, a linear dynamic range (LDR) of 0.5–15 μM with an R^2 of 0.9995, sensitivity of 11.9 ± 0.1 μA μM^{-1}, limit of detection (LOD) of 0.138 μM and limit of quantification (LOQ) of 0.461 μM were obtained. The LOD and LOQ were calculated based on the IUPAC definition (LOD $= 3\sigma/s$ and LOQ $= 10\sigma/s$) where σ is the standard deviation of the baseline noise and s is the analytical sensitivity of the calibration curve [47]. The performance of the proposed AM genosensor was compared to other biosensors reported in the literature for the diagnosis of Yellow Fever Virus, as shown in Table 3 [48–51] which shows our proposed sensor compares well.

The specificity of the proposed system using L-COOH-MWCNT was tested after the hybridization reaction with 10 μM Yellow Fever virus cDNA and 10 μM Dengue virus cDNA as the negative target, Fig. 6B and S4A. It can be seen that there was no significant change in the measured peak current for the incubation with Dengue virus cDNA, and a large decrease from 192 ± 18 μA to 88 ± 6 μA when the sensing platform was incubated with Yellow Fever virus cDNA. This proves that negative targets have no complementary hybridization with the YFV capture
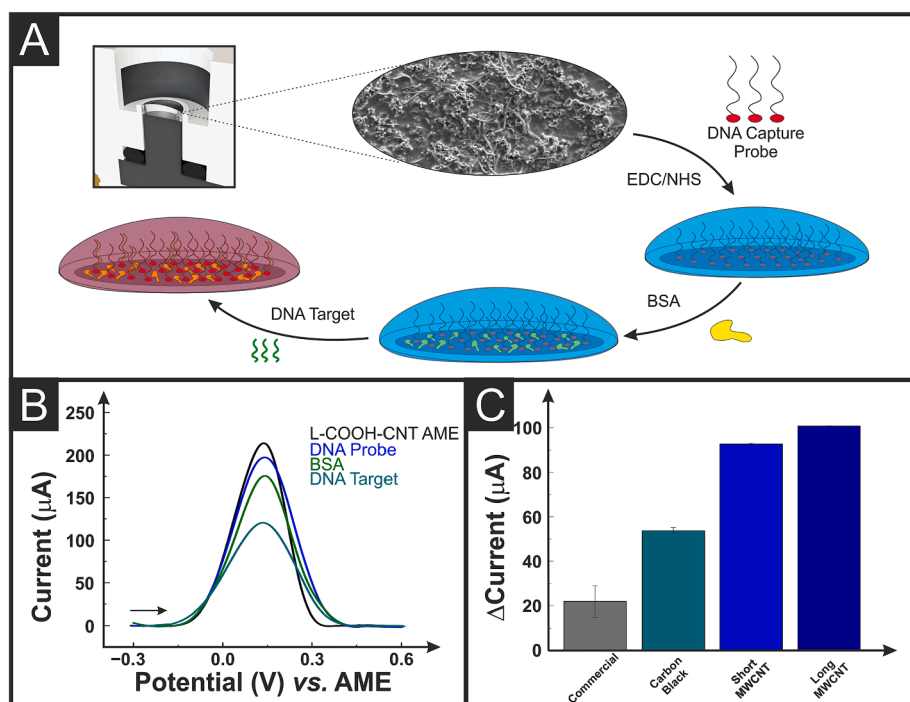

Fig. 5. A) Schematic representation of the genosensor production by drop-casting: immobilization of the DNA capture probe by using EDC/NHS, BSA for nonspecific interactions, and cDNA hybridization reaction. **B)** Square wave voltammetric tracking of the different immobilisation steps. **C)** Plot showing the overall change in peak current obtained when performing the immobilisations steps on electrodes made from each of the four filaments.
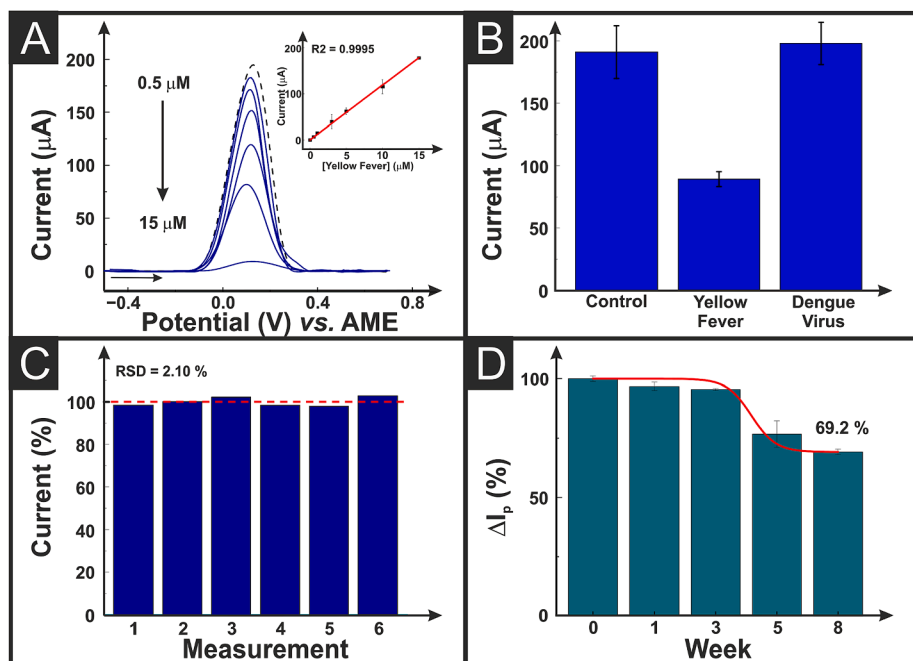
Fig. 6. A) Anodic square wave voltammograms corresponding to the detection of Yellow Fever virus cDNA using the AM genosensor with a working electrode using the long-COOH-MWCNT filament. B) Selectivity plot showing the change in peak current obtained in the presence of Yellow Fever virus, Dengue virus and a control using the long-COOH-MWCNT filament. C) Reproducibility study for the detection of 1 µM Yellow Fever virus cDNA onto six different AMEs from the long-COOH-MWCNT filament. D) Stability study for the detection of 1 µM Yellow Fever virus cDNA onto the genosensor between 1 and 8 weeks. (For interpretation of the references to colour in this figure legend, the reader is referred to the web version of this article.)

Table 3
Comparison of the performance of the produced additive manufacturing genosensor to other yellow fever virus biosensors in the literature.

Assay/Probe	Target	Technique	LDR	LOD	Ref.
Lateral flow strips with conjugate pads loaded with Ag NPs / Anti-YFV NS1 antibodies	NS1 protein	Colorimetry	0–500 ng mL^{-1}	150 ng mL^{-1}	[51]
Paper-based device using a screen-printed carbon electrode decorated with ZnO NPs / YFV DNA	YFV DNA	Cyclic Voltammetry	0.01–100 µM	0.01 µM	[48]
Self-assembled monolayer based on a gold electrode decorated with ZnO NPs / Concanavalin A lectin	YFV attenuated vaccine strain	Electrochemical Impedance Spectroscopy	0.036–0.18 pfu mL^{-1}	0.0437 pfu mL^{-1}	[52]
Sandwich enzyme-linked oligonucleotide assay / YF NS1-31 capture aptamer	YFV-NS1 aptamers	Spectroscopy / Colorimetry	1.56–200 nM	0.85 nM	[49]
3D r-PLA/CB/L-COOH-MWCNT / YFV DNA	*YFV cDNA*	*Square Wave Voltammetry*	*0.5–15 µM*	*0.138 µM*	*This work*

sequence; thus, the proposed genosensor showed a specific detection for Yellow Fever virus cDNA target. Furthermore, the repeatability was tested through measuring six separate sensing platforms with the incubation of 1 µM Yellow Fever virus cDNA, Fig. 6C. It can be seen that using the ASWV methodology an RSD of 2.10% (n = 6) was obtained, highlighting the reliability of the system. The stability over time of the system was also investigated, with measurements taken 1, 2, 4, 6 and 8 weeks after biosensor production, stored at 4 °C. There is minimal decrease in the measured currents for the first 4 weeks, and then a decrease to 69.2% of the original genosensor response 8 weeks after production. This highlights the stability of the proposed genosensor platform. This combined with the ability to print sensors anywhere with power for a print and the facile droplet production methodology would allow these genosensor platforms to be produced in low-resource environments. The proposed L-COOH-MWCNT additive manufacturing

genosensor was then tested toward the detection of Yellow Fever virus target sequence in spiked human serum samples, presented in Table 4 and Figure S4B. This was tested in triplicate with three separate concentrations of spiked Yellow Fever virus cDNA. The proposed additive manufacturing genosensor platform obtained good recovery values of 95.6–105%, highlighting the applicability of the biosensor.

The development of a new additive manufacturing filament containing carboxylated MWCNT and its application to the facile production of genosensors has the potential to transform the global response to future disease outbreaks. It combines the advantages of additive manufacturing, where the design of sensors can be completed anywhere in the world and produced in-situ through transferring the print file, and the benefits of facile droplet modification where no skilled production staff are required. We foresee this technology being translated into use for other biorecognition elements and applications, enabling disease monitoring in point-of-care devices such as for sepsis, and emergent or cardiac diseases.

4. Conclusions

This work describes the production of bespoke conductive additive manufacturing feedstock from recycled PLA embedded with carboxylated multi-walled carbon nanotubes. The unique composition of this filament - comprising of 65 wt% rPLA, 10 wt% PES, 15 wt% CB, and 10 wt% L-COOH-MWCNT - allows for the facile production of a genosensor

Table 4
Detection of Yellow Fever virus cDNA in spiked human serum. Uncertainties in the values represent the standard deviation from three separate measurements.

	Added (µM)	Found (µM)	Recovery (%)	RSD (%)
Human Serum Sample	1.00	1.05 ± 0.12	105	4.71
	5.00	5.11 ± 1.06	102	2.17
	10.0	9.56 ± 1.95	95.6	4.38

through simply applying droplets to the working electrode surface, held in place by the bespoke AM electroanalytical cell. This droplet modification is extended to the activation of the AME, which historically has been done through electrochemical means. The filament exhibited a significantly enhanced electrochemical performance with a measured k^0 of $(1.85 \pm 0.42) \times 10^{-3}$ cm s^{-1} and an electrochemically active area of (2.11 ± 0.03) cm^2 compared to $(1.19 \pm 0.19) \times 10^{-3}$ cm s^{-1}, and (1.35 ± 0.02) cm^2 for an identical AME printed with the commercial filament. When the assembled genosensor was applied to the detection of Yellow Fever virus target sequence using anodic square wave voltammetry, a linear dynamic range (LDR) of 0.5–15 μM was obtained with an R^2 of 0.9995, sensitivity of 11.9 ± 0.1 μA μM^{-1}, and limit of detection (LOD) of 0.14 μM. Additionally, the L-COOH-MWCNT AM genosensor provided excellent selectivity when Dengue virus sequences were used. Over multiple measurements, the genosensor achieved impressive reproducibility with an RSD of just 2.10% and maintained 95% of the original signal 4 weeks after production. The system was successfully applied to the detection of Yellow Fever virus target sequence within human blood serum samples, achieving recoveries between 95.6 and 105%. This work shows how bespoke filament can be produced for additively manufactured electrochemical biosensors, enhancing the recognition element binding and electrochemical performance of the sensor. Additive manufacturing allows for the design of these devices anywhere, with the print then able to be produced at the site where needed most. We expect the use of this filament and filaments with further modified advanced materials to help additive manufacturing electrochemistry realise its potential in the global healthcare field.

Declaration of Competing Interest

The authors declare that they have no known competing financial interests or personal relationships that could have appeared to influence the work reported in this paper.

Data availability

Data will be made available on request.

Acknowledgements

Appendix A. Supplementary data

Supplementary data to this article can be found online at https://doi.org/10.1016/j.cej.2023.143513.

References

[1] O. Vandenberg, D. Martiny, O. Rochas, A. van Belkum, Z. Kozlakidis, Considerations for diagnostic COVID-19 tests, Nat. Rev. Microbiol. 19 (3) (2021) 171–183, https://doi.org/10.1038/s41579-020-00461-z.

[2] M.J. Whittingham, R.D. Crapnell, E.J. Rothwell, N.J. Hurst, C.E. Banks, Additive manufacturing for electrochemical labs: An overview and tutorial note on the production of cells, electrodes and accessories, Talanta Open 4 (2021), 100051, https://doi.org/10.1016/j.talo.2021.100051.

[3] A.-G.-M. Ferrari, N.J. Hurst, E. Bernalte, R.D. Crapnell, M.J. Whittingham, D. A. Brownson, C.E. Banks, Exploration of defined 2-dimensional working electrode shapes through additive manufacturing, Analyst 147 (22) (2022) 5121–5129, https://doi.org/10.1039/D2AN01412B.

[4] M.J. Whittingham, R.D. Crapnell, C.E. Banks, Additively manufactured rotating disk electrodes and experimental setup, Anal. Chem. 94 (39) (2022) 13540–13548, https://doi.org/10.1021/acs.analchem.2c02884.

[5] P. Wuamprakhon, R.D. Crapnell, E. Sigley, N.J. Hurst, R.J. Williams, M. Sawangphruk, E.M. Keefe, C.E. Banks, Recycled Additive Manufacturing Feedstocks for Fabricating High Voltage, Low-Cost Aqueous Supercapacitors, Adv. Sustain. Syst. 7 (2) (2023) 2200407.

[6] E. Sigley, C. Kalinke, R.D. Crapnell, M.J. Whittingham, R.J. Williams, E.M. Keefe, B.C. Janegitz, J.A. Bonacin, C.E. Banks, Circular Economy Electrochemistry: Creating Additive Manufacturing Feedstocks for Caffeine Detection from Post-Industrial Coffee Pod Waste, ACS Sustain. Chem. Eng. 11 (7) (2023) 2978–2988.

[7] Nations, U. Sustainable Development Goals. https://sdgs.un.org/goals (accessed 14/10/2022).

[8] B. Huang, C. Vyas, I. Roberts, Q.-A. Poutrel, W.-H. Chiang, J.J. Blaker, Z. Huang, P. Bártolo, Fabrication and characterisation of 3D printed MWCNT composite porous scaffolds for bone regeneration, Mater. Sci. Eng. C 98 (2019) 266–278, https://doi.org/10.1016/j.msec.2018.12.100.

[9] N. Vidakis, M. Petousis, E. Velidakis, L. Tzounis, N. Mountakis, O. Boura, S. A. Grammatikos, Multi-functional polyamide 12 (PA12)/multiwall carbon nanotube 3D printed nanocomposites with enhanced mechanical and electrical properties, Adv. Compos. Mater 31 (6) (2022) 630–654, https://doi.org/10.1080/09243046.2022.2076019.

[10] E. Ivanov, R. Kotsilkova, H. Xia, Y. Chen, R. Donato, K. Donato, A. Godoy, R. Di Maio, C. Silvestre, S. Cimmino, V. Angelov, PLA/Graphene/MWCNT composites with improved electrical and thermal properties suitable for FDM 3D printing applications, Appl. Sci. 9 (6) (2019) 1209.

[11] Proto-pasta Composite Conductive Fiber PLA (CDP1xxxx). https://cdn.shopify.com/s/files/1/0717/9095/files/CDP1xxxx_SDS.pdf?1992606272897634343 (accessed 17/08/2022).

[12] K. Ghosh, S. Ng, C. Iffelsberger, M. Pumera, 2D MoS2/carbon/polylactic acid filament for 3D printing: photo and electrochemical energy conversion and storage, Appl. Mater. Today 26 (2022), 101301, https://doi.org/10.1016/j.apmt.2021.101301.

[13] R.D. Crapnell, N.C. Dempsey, E. Sigley, A. Tridente, C.E. Banks, Electroanalytical point-of-care detection of gold standard and emerging cardiac biomarkers for stratification and monitoring in intensive care medicine-a review, Microchim. Acta 189 (4) (2022) 1–48, https://doi.org/10.1007/s00604-022-05186-9.

[14] A. Florea, G. Melinte, I. Simon, C. Cristea, Electrochemical biosensors as potential diagnostic devices for autoimmune diseases, Biosensors 9 (1) (2019) 38, https://doi.org/10.3390/bios9010038.

[15] Y. Huang, J. Xu, J. Liu, X. Wang, B. Chen, Disease-related detection with electrochemical biosensors: A review, Sensors 17 (10) (2017) 2375, https://doi.org/10.3390/s17102375.

[16] S. Menon, M.R. Mathew, S. Sam, K. Keerthi, K.G. Kumar, Recent advances and challenges in electrochemical biosensors for emerging and re-emerging infectious diseases, J. Electroanal. Chem. 878 (2020), 114596, https://doi.org/10.1016/j.jelechem.2020.114596.

[17] S. Taniselass, M.M. Arshad, S.C. Gopinath, Graphene-based electrochemical biosensors for monitoring noncommunicable disease biomarkers, Biosens. Bioelectron. 130 (2019) 276–292, https://doi.org/10.1016/j.bios.2019.01.047.

[18] L.C. Brazaca, P.L. Dos Santos, P.R. de Oliveira, D.P. Rocha, J.S. Stefano, C. Kalinke, R.A.A. Munoz, J.A. Bonacin, B.C. Janegitz, E. Carrilho, Biosensing strategies for the electrochemical detection of viruses and viral diseases–A review, Anal. Chim. Acta 1159 (2021), 338384, https://doi.org/10.1016/j.aca.2021.338384.

[19] H.A.M. Faria, V. Zucolotto, Label-free electrochemical DNA biosensor for zika virus identification, Biosens. Bioelectron. 131 (2019) 149–155, https://doi.org/10.1016/j.bios.2019.02.018.

[20] P. Sharma, S. Suleman, A. Farooqui, W. Ali, J. Narang, S.J. Malode, N.P. Shetti, Analytical methods for Ebola virus detection, Microchem. J. 178 (2022), 107333, https://doi.org/10.1016/j.microc.2022.107333.

[21] S.A. Abid, A.A. Muneer, I.M. Al-Kadmy, A.A. Sattar, A.M. Beshbishy, G.-E.-S. Batiha, H.F. Hetta, Biosensors as a future diagnostic approach for COVID-19, Life Sci. 273 (2021), 119117, https://doi.org/10.1016/j.lfs.2021.119117.

[22] G. Balkourani, A. Brouzgou, M. Archonti, N. Papandrianos, S. Song, P. Tsiakaras, Emerging materials for the electrochemical detection of COVID-19, J. Electroanal. Chem. 893 (2021), 115289, https://doi.org/10.1016/j.jelechem.2021.115289.

[23] J. Kudr, P. Michalek, L. Ilieva, V. Adam, O. Zitka, COVID-19: A challenge for electrochemical biosensors, TrAC Trends Anal. Chem. 136 (2021), 116192, https://doi.org/10.1016/j.trac.2021.116192.

[24] A.D. Luong, A. Buzid, S.K. Vashist, J.H. Luong, Perspectives on electrochemical biosensing of COVID-19, Curr. Opin. Electrochem. 30 (2021), 100794, https://doi.org/10.1016/j.coelec.2021.100794.

[25] S.S. Mahshid, S.E. Flynn, S. Mahshid, The potential application of electrochemical biosensors in the COVID-19 pandemic: A perspective on the rapid diagnostics of SARS-CoV-2, Biosens. Bioelectron. 176 (2021), 112905, https://doi.org/10.1016/j.bios.2020.112905.

[26] V. Van Tran, N.H.T. Tran, H.S. Hwang, M. Chang, Development strategies of conducting polymer-based electrochemical biosensors for virus biomarkers: Potential for rapid COVID-19 detection, Biosens. Bioelectron. 182 (2021), 113192, https://doi.org/10.1016/j.bios.2021.113192.

[27] A. Yakoh, U. Pimpitak, S. Rengpipat, N. Hirankarn, O. Chailapakul, S. Chaiyo, paper based electrochemical biosensor for diagnosing COVID-19: Detection of SARS-CoV-2 antibodies and antigen, Biosens. Bioelectron. 176 (2021), 112912, https://doi.org/10.1016/j.bios.2020.112912.

[28] Blasques, R. V.; Oliveira, P. R. d.; Kalinke, C.; Brazaca, L. C.; Crapnell, R. D.; Bonacin, J. A.; Banks, C. E.; Janegitz, B. C. Flexible Label-Free Platinum and Bio-PET-Based Immunosensor for the Detection of SARS-CoV-2. *Biosensors* **2023,** *13* (2), 190, doi: 10.3390/bios13020190.

[29] N. Kumar, N.P. Shetti, S. Jagannath, T.M. Aminabhavi, Electrochemical sensors for the detection of SARS-CoV-2 virus, Chem. Eng. J. 430 (2022), 132966, https://doi.org/10.1016/j.cej.2021.132966.

[30] S.D. Bukkitgar, N.P. Shetti, T.M. Aminabhavi, Electrochemical investigations for COVID-19 detection-A comparison with other viral detection methods, Chem. Eng. J. 420 (2021), 127575, https://doi.org/10.1016/j.cej.2020.127575.

[31] S. Suleman, S.K. Shukla, N. Malhotra, S.D. Bukkitgar, N.P. Shetti, R. Pilloton, J. Narang, Y. Nee Tan, T.M. Aminabhavi, Point of care detection of COVID-19: Advancement in biosensing and diagnostic methods, Chem. Eng. J. 414 (2021), 128759, https://doi.org/10.1016/j.cej.2021.128759.

[32] Organisation, W. H. Yellow fever - African Region (AFRO). https://www.who.int/emergencies/disease-outbreak-news/item/2022-DON431 (accessed 08/02/2023).

[33] Fenollar, F.; Mediannikov, O. Emerging infectious diseases in Africa in the 21st century. *New Microbes and New Infections* **2018,** *26*, S10-S18, doi: 10.1016/j.nmni.2018.09.004.

[34] T.P. Monath, P.F.C. Vasconcelos, Yellow fever, Yellow fever. *Journal of clinical virology* 64 (2015) 160–173.

[35] T.P. Monath, E. Fowler, C.T. Johnson, J. Balser, M.J. Morin, M. Sisti, D.W. Trent, An inactivated cell-culture vaccine against yellow fever, N. Engl. J. Med. 364 (14) (2011) 1326–1333, https://doi.org/10.1056/NEJMoa1009303.

[36] G. Greczynski, L. Hultman, The same chemical state of carbon gives rise to two peaks in X-ray photoelectron spectroscopy, Sci. Rep. 11 (1) (2021) 1–5, https://doi.org/10.1038/s41598-021-90780-9.

[37] R.J. Williams, T. Brine, R.D. Crapnell, A.-G.-M. Ferrari, C.E. Banks, The effect of water ingress on additively manufactured electrodes, Materials Advances 3 (20) (2022) 7632–7639, https://doi.org/10.1039/D2MA00707J.

[38] X. Wang, Y. Zhuang, L. Dong, Study of carbon black-filled poly (butylene succinate)/polylactide blend, J. Appl. Polym. Sci. 126 (6) (2012) 1876–1884, https://doi.org/10.1002/app.36944.

[39] Y.-H. Zhao, Y.-F. Zhang, Z.-K. Wu, S.-L. Bai, Synergic enhancement of thermal properties of polymer composites by graphene foam and carbon black, Compos. B Eng. 84 (2016) 52–58, https://doi.org/10.1016/j.compositesb.2015.08.074.

[40] J. Guo, C.-H. Tsou, Y. Yu, C.-S. Wu, X. Zhang, Z. Chen, T. Yang, F. Ge, P. Liu, M.R. D. Guzman, Conductivity and mechanical properties of carbon black-reinforced poly (lactic acid)(PLA/CB) composites, Iran. Polym. J. 30 (12) (2021) 1251–1262, https://doi.org/10.1007/s13726-021-00973-2.

[41] R.D. Crapnell, A. Garcia-Miranda Ferrari, M.J. Whittingham, E. Sigley, N.J. Hurst, E.M. Keefe, C.E. Banks, Adjusting the Connection Length of Additively Manufactured Electrodes Changes the Electrochemical and Electroanalytical Performance, Sensors 22 (23) (2022) 9521, https://doi.org/10.3390/s22239521.

[42] R.D. Crapnell, E. Bernalte, A.-G.-M. Ferrari, M.J. Whittingham, R.J. Williams, N. J. Hurst, C.E. Banks, All-in-one single-print additively manufactured electroanalytical sensing platforms, ACS Measurement Science Au 2 (2) (2021) 167–176, https://doi.org/10.1021/acsmeasuresciau.1c00046.

[43] P. Delhaes, M. Couzi, M. Trinquecoste, J. Dentzer, H. Hamidou, C. Vix-Guterl, A comparison between Raman spectroscopy and surface characterizations of multiwall carbon nanotubes, Carbon 44 (14) (2006) 3005–3013, https://doi.org/10.1016/j.carbon.2006.05.021.

[44] F. Tuinstra, J. Koenig, Characterization of graphite fiber surfaces with Raman spectroscopy, J. Compos. Mater. 4 (4) (1970) 492–499, https://doi.org/10.1177/002199837000400405.

[45] R.L. McCreery, Advanced carbon electrode materials for molecular electrochemistry, Chem. Rev. 108 (7) (2008) 2646–2687, https://doi.org/10.1021/cr068076m.

[46] A. García-Miranda Ferrari, C.W. Foster, P.J. Kelly, D.A. Brownson, C.E. Banks, Determination of the electrochemical area of screen-printed electrochemical sensing platforms, Biosensors 8 (2) (2018) 53, https://doi.org/10.3390/bios8020053.

[47] Long, G. L.; Winefordner, J. D. Limit of detection. A closer look at the IUPAC definition. *Analytical chemistry* **1983,** *55* (7), 712A-724A, doi: 10.1021/ac00258a724.

[48] N.K. Mehto, P. Sharma, S. Kumar, M. Khanuja, R. Rawal, J. Narang, Towards papertronics based electrode decorated with zinc oxide nanoparticles for the detection of the yellow fever virus consensus sequence, Process Biochem. 123 (2022) 36–43, https://doi.org/10.1016/j.procbio.2022.10.026.

[49] J. Mok, E. Kim, M. Kang, J. Jeon, C. Ban, Development of an optical sandwich ELONA using a pair of DNA aptamers for yellow fever virus NS1, Talanta 253 (2023), 123979, https://doi.org/10.1016/j.talanta.2022.123979.

[50] E.P. Simão, D.B. Silva, M.T. Cordeiro, L.H. Gil, C.A. Andrade, M.D. Oliveira, Nanostructured impedimetric lectin-based biosensor for arboviruses detection, Talanta 208 (2020), 120338, https://doi.org/10.1016/j.talanta.2019.120338.

[51] C.-W. Yen, H. de Puig, J.O. Tam, J. Gómez-Márquez, I. Bosch, K. Hamad-Schifferli, L. Gehrke, Multicolored silver nanoparticles for multiplexed disease diagnostics: distinguishing dengue, yellow fever, and Ebola viruses, Lab Chip 15 (7) (2015) 1638–1641, https://doi.org/10.1039/C5LC00055F.